

# CHALMERS



## Using USRP in Reverberation Chamber for studying throughput

*Master of Science Thesis in Communication Engineering*

**BJARNI Þ. EINARSSON**

Department of Signals and Systems  
*Antenna Systems Division*

CHALMERS UNIVERSITY OF TECHNOLOGY  
Gothenburg, Sweden, 2014  
Report No. EX016/2014

# Using USRP in Reverberation Chamber for studying throughput

Bjarni Þór Einarsson

©Bjarni Þór Einarsson, 2014

Department of Signals and Systems  
Chalmers University of Technology  
SE-412 96 Göteborg  
Sweden  
Telephone + 46 (0)31-772 1000

Göteborg, Sweden 2014

# Summary

The purpose of the project is to validate that universal software radio peripherals (USRP) can be used in conjunction with a reverberation chamber (RC) in order to measure the quality of communication system accurately over the rich isotropic multipath channel (RIMP), e.g. throughput and total isotropic sensitivity. The reason behind using USRP and not any standardized communication device is that we can reduce the cost, and at the same time do more advanced tests by getting access to the whole system. With added complexity the systems have more and more unknowns giving them more of a black box property than a proper test bench where a researcher can implement his own algorithm and test them in a measurement environment to check if they follow theoretical models. This is in contrast to proprietary built-in algorithms implemented on the device under test (DUT). The USRP provides an inexpensive and quite reliable radio platform that is needed in order to test the performance of the communication system under test [1]

In the first part of the project the single bit stream throughput cases; single input, single output (SISO) and multiple input, multiple output (MIMO) with transmit and receive diversity and related algorithms, i.e. selection combining (SC) and maximum ratio combining (MRC), are examined. Both conductive measurements and over-the-air (OTA) measurements are performed. All measured OTA throughput shows good agreement with the theoretical throughput for the RIMP in the first part of the project. The RIMP environment is accurately emulated by a reverberation chamber and is a useful reference channel for measuring wireless devices [3], and the threshold receiver model presented in [2].

In the second part of the project a further study of throughput is conducted for the MIMO throughput case for both single and double bit stream cases. Furthermore the capabilities of a USRP as a measuring instrument are examined using SISO measurement setup to perform active measurements such as total radiated power (TRP), total isotropic sensitivity (TIS), and throughput. The passive tests of antenna efficiency, correlation, and diversity gain were also performed using USRP. In a direct continuation of that, the capabilities of the USRP for measuring channel parameters such as Doppler spread and root mean square (RMS) Delay spread are also investigated.

The measurement results show that nearly all measurements agree with the expected theoretical values within 1dB offset for nearly all tests giving a strong indication that the USRP can be used as a test bench for more complex algorithms and communication links.

Keywords: USRP, Universal Software Radio Peripheral, RC, Reverberation Chamber, Throughput, Rich Isotropic Multipath, RIMP, Total Isotropic sensitivity, TIS, Antenna Efficiency, RMS Delay Spread, Total Radiated Power, TRP

## Preface

This is the final report on the master's thesis work performed by Bjarni Þór Einarsson for a Master of Science degree in Communication Engineering. Work was done at the Antenna Systems Division which belongs to the Signals and Systems department of Chalmers from September 2013 to May 2014. The work was performed under the primary supervision of Ahmed Hussain and secondary supervision of Chen Xiaoming. Examiner was Per-Simon Kildal.

The report writer would like to thank Payman Tehrani from National Instruments for his support in the early phases of the work and both supervisors Ahmed and Chen for their discussions and ideas on the work performed.

# Contents

1 Introduction.....	6
2 Theory.....	7
2.1 Threshold receiver model.....	7
2.2 Rich isotropic multipath channel.....	7
2.3 Combining methods.....	7
2.4 Alamouti algorithm.....	9
2.5 Zero forcing.....	9
2.6 Singular value decomposition.....	10
2.7 Theoretical throughput.....	11
2.8 Total isotropic sensitivity.....	12
2.9 Total radiated power.....	12
2.10 Radiation efficiency.....	13
2.11 Doppler spread.....	13
2.12 Delay spread.....	14
3 System description.....	15
3.1 Detailed system description.....	17
3.1.1 Packet transmitter.....	17
3.1.2 Packet receiver.....	18
3.1.3 Transmitter and receiver.....	18
3.2 Limitations.....	19
4 Measurement setup & results.....	20
4.1 Throughput measurements.....	20
4.1.1 Single input, single output (SISO).....	21
4.1.2 Multiple input, single output (MISO).....	23
4.1.3 Single input, multiple output (SIMO).....	23
4.1.4 Multiple input, multiple output (MIMO).....	24
4.2 System Parameters.....	27
4.2.1 NI USRP N210 properties.....	28
4.2.2 Total isotropic sensitivity (TIS).....	30
4.2.3 Total radiated power (TRP).....	30
4.2.4 Efficiency.....	31
4.2.5 Diversity gain & correlation.....	32
4.3 Channel properties.....	35
4.3.1 Doppler spread.....	35
4.3.2 Delay spread.....	35
6 Conclusions.....	37
7 References.....	38

# 1 Introduction

With increasing complexity of commercial digital wireless systems used in modern wireless telecommunications the cost of reliable testing platforms increases. Therefore, the demand for simple and cost effective measurement platforms is increasing. Those platforms must be capable of measuring and quantifying the performance of both new hardware and new algorithms, with no exception to simplified theoretical system models. The universal software radio peripheral (USRP) fits that demand well as it is both inexpensive and versatile as it can be used to implement and test most modern algorithms in practice [1]. The reverberation chamber (RC) has been proven to accurately emulate the rich isotropic multipath channel (RIMP), which is a useful reference channel for modern wireless communication devices that do not operate in line of sight [3].

The purpose of this project is to demonstrate that the USRP can be used in conjunction with the RC in order to accurately measure relative system throughput and other related system parameters. First for simple systems (i.e. single bit stream SISO up to 2x2 MIMO) and later for more complex systems (i.e. double bit stream) over the RIMP. The results from which can be shown to be in agreement with the threshold receiver model presented in [2] and theories based on it. Furthermore the capabilities of the USRP to perform various system and channel measurements are investigated and compared with results from a vector network analyzer (VNA) and spectrum analyzer (SA).

It has been well proven that the RC measurements are accurate [9] and shown to be in agreement with results for passive devices in the anechoic chambers [10]-[11].

Additionally, the RC is capable of emulating different delay spreads [12] making it possible to measure the effects of changed delay spread in OFDM and active devices. The measured results for different delay spreads are in good agreement with the threshold receiver model in [2]. Meaning the effects of different delay spreads that effect OFDM in LTE systems can be measured and has been modelled in [13]. Further work has additionally been done to extend the threshold receiver model to the MIMO multiplexing case [14]

In the first part of the project the single bit stream case with simple algorithms has been successfully implemented and measured to be in good agreement with the threshold model, both for SISO [3] and up to 2x2 MIMO [14], results from which are presented in this report.

In the second part of the project single bit stream Alamouti algorithm and double bit stream systems implementing zero forcing (ZF) and singular value decomposition (SVD) were implemented and measured. Where the implementation was successful the results are in good agreement with the threshold receiver model for the 2x2 MIMO.

Furthermore algorithms were implemented to measure antenna efficiency, total radiated power (TRP) of devices, total isotropic sensitivity (TIS), diversity gain and perform self-measurements on the USRP and the channel it is transmitting over for measuring RMS delay spread and Doppler spread whose values were found in most cases to be in good agreement with theoretical and VNA measured reference values with the exception of the Doppler spread and diversity gain.

## 2 Theory

The project combines many methods and models that come together to accurately model the communication links and models that are tested. This chapter will describe the main principles used in this project.

### 2.1 Threshold receiver model

The most basic assumption of the system in order to predict the throughput of the system as a function of received power is the threshold receiver model that states that the throughput for the AWGN channel can be expressed as a function of the group error rate (GER) or packet error (PER) [2]. For this the GER can be defined as

$$GER(P) = \begin{cases} 1, & P < P_t \\ 0, & P > P_t \end{cases} \quad (1)$$

Where  $P$  is the received power and  $P_t$  is the threshold power of the receiver. This can be extended to throughput as (2) where  $Maxrate$  is the maximum possible throughput.

$$Throughput = Maxrate * \{1 - GER(P)\} \quad (2)$$

Following that the threshold receiver model can be extended for more complex systems and channels with the knowledge of the cumulative distribution function (CDF) of the received power after signal processing in terms of

$$GER_{av}(P_{av}) = CDF\left(\frac{P_t}{P_{av}}\right) \quad (3)$$

Where  $P_{av}$  is the average received power. Substituting (3) for the GER in (2) we can then use (2) as a general expression for the throughput as the CDFs inside the chamber can be readily estimated from simulations.

### 2.2 Rich isotropic multipath channel

The RIMP is accurately emulated by the RC and is a useful reference channel for most modern communication devices [3]. The characterization of which is best described by the uniform angle of arrival over all directions in space. Due to this property the DUT becomes statistically independent of its orientation in space. This provides the DUT with arbitrary polarization, amplitude, phase and time variation of the received signal.

By selecting a sufficiently large RC compared to the maximum wavelength of the system under test it can achieve a significantly large amount of wave modes achieving the properties described above, giving the received power a Rayleigh distribution.

### 2.3 Combining methods

In order to achieve receiver diversity a method is needed for processing the received signal. In this project two methods are primarily used, selection combining (SC) and maximum ratio combining (MRC) [19]. Those combining methods have been implemented successfully for any system in this project that has two receiving ports or more.

Denoting the  $k$ -th received streams  $l$ -th sample as (4) assuming zero noise for any received sample  $y$ .

$$y_l^k = \alpha_l \cdot e^{j\beta_l} \cdot s_l \quad (4)$$

Here  $\alpha$  denotes the instantaneous amplitude and  $\beta$  denotes the instantaneous phase of the received sample and  $s$  denotes the transmitted symbol.

Selection combining is the simpler of the two methods and has the advantage of being more computationally efficient and has the notation as follows for the instantaneous power in the l-th sample according to

$$|y_l|^2 = \max(|y_l^1|^2, |y_l^2|^2) \quad (5)$$

Where  $y_l$  denotes the l-th sample chosen from one of the k bit streams denoted by  $y^k$  ( $k=1, 2$ ). The algorithm chooses the higher power sample at each sampling instant giving an expected diversity gain of

$$Gain = \sum_{k=1}^N \frac{1}{k} \quad (6)$$

N here is the total number of receiver streams

Maximum ratio combining requires more information and computation than selection combining but achieves a higher diversity gain or

$$Gain = \sum_{k=1}^N SNR_k \quad (7)$$

Where  $SNR_k$  denotes the k-th received signal to noise ratio. To achieve this diversity gain the receiver must know the channel state information (CSI) in order to estimate the phase and amplitude of the channel affecting the signal. Given that the notation for the instantaneous power becomes (8) after phase and amplitude correction

$$|y_l|^2 = |y_l^1|^2 + |y_l^2|^2 \quad (8)$$

The estimation of the phase and amplitude is done by transmitting a bit sequence known to both the transmitter (TX) and receiver (RX). By knowing the training sequence the receiver can then estimate the channel by de-convoluting the channel response from the received sequence. In this project that is done by the following steps after isolating the training sequence from the received packet:

$$F\{t\} = T \quad (9)$$

$$F\{h * t\} = HT \quad (10)$$

$$\tilde{h} = F^{-1}\{HT/T\} \quad (11)$$

$$\tilde{h} = \tilde{\alpha}e^{j\tilde{\beta}} \quad (12)$$

Here the  $F\{t\}$  operation denotes the Fourier transform of  $t$  and  $*$  denotes convolution. In (9)  $t$  denotes the training sequence at the receiver side (length  $m$ ) and in (10)  $h * t$  denotes the received training sequence after transmission through the channel  $h$ . In (11)  $\tilde{h}$  denotes the channel estimate given in terms of its phase and amplitude in (12). By multiplying the conjugate of (12) with (4) we can then receive the phase and amplitude corrected instantaneous sample we get

$$\widetilde{y}_j^k = \alpha^2 s_j \quad (13)$$

This is done under the assumption that the channel estimate is valid for the entire length of the transmitted packet.

## 2.4 Alamouti algorithm

The Alamouti algorithm as explained in [5] provides a way for improved antenna diversity without added bandwidth or reduced bitrate of a single bit stream. For 2 transmit antennas and M receiver antennas it provides a diversity order of 2M for the same bandwidth as a single bit stream. For any case where there are 2 transmitters the same transmission matrix (14) is used for interleaving in time between the antennas.

$$\begin{bmatrix} s_0 & s_1 \\ -s_1^* & s_0^* \end{bmatrix} \quad (14)$$

Here  $s_0$  denotes the first symbol for transmission, and  $s_1$  denotes the second symbol. This pattern repeats itself with the third symbol then taking the place of  $s_0$  and so on. This interleaving in time is done so that at the receiver side (15) can be achieved as follows for 2x1 MISO and (16) for 2x2 MIMO

$$\begin{aligned} y_0 &= h_0 r_0 + h_1 r_1 \\ y_1 &= -h_0 r_1^* + h_1 r_0^* \end{aligned} \quad (15)$$

$$\begin{aligned} y_0 &= h_0^* r_0 + h_1 r_1^* + h_2^* r_2 + h_3 r_3^* \\ y_1 &= h_1^* r_0 - h_0 r_1^* + h_3^* r_2 - h_2 r_3^* \end{aligned} \quad (16)$$

Here  $r_l$  denotes the l-th symbol received in time. For the 2x2 case the two parallel channels count (1, 2) and (3, 4) on the two consecutive time instants.

Using the notation in (4) and (13) the instantaneous received power for the Alamouti algorithm for MISO becomes

$$\tilde{y}_l = (\alpha_0^2 + \alpha_1^2) s_l \quad (17)$$

Where  $\alpha_k$  denotes the k-th channels amplitude. This can be expanded with ease to the 2x2 MIMO for an instantaneous power of (18) for each receiver channel

$$\tilde{y}_l = (\alpha_0^2 + \alpha_1^2 + \alpha_2^2 + \alpha_3^2) s_l \quad (18)$$

Effectively using MRC for all four channels of the 2x2 channel matrix rather than a combination of only two if MRC were used for the 2x2 MIMO system.

## 2.5 Zero forcing

In order to achieve two bit streams on the same bandwidth using a 2x2 MIMO system the zero forcing algorithm is used as it provides a relatively simple mathematical solution using the pseudo inverse of the channel matrix as defined in [20] as

$$\mathbf{H}^\dagger = (\mathbf{H}\mathbf{H})^{-1}\mathbf{H}^* \quad (19)$$

Here  $\mathbf{H}$  denotes the channel state matrix as estimated by the receiver. If the CSI is perfect at the receiver it can be shown to achieve double the throughput of the single bit stream [6]. In order to decorrelate the channels the pseudo inverse channel matrix  $\mathbf{H}^\dagger$  is multiplied with the received waveforms and the product is the two separate bit streams ready for demodulation.

## 2.6 Singular value decomposition

Singular value decomposition (SVD) is used in order to achieve beam forming by precoding the transmitted waveform using CSI at the transmitter. Assuming the channel matrix  $\mathbf{H}$  has full rank then the number of independent bit streams without inter symbol interference can be equal to its rank. In order to precode the singular value decomposition of  $\mathbf{H}$  must be done, which is defined in [20] as

$$\mathbf{H} = \mathbf{U}\mathbf{\Lambda}\mathbf{V}^H \quad (20)$$

$$\mathbf{U}^H\mathbf{U} = \mathbf{U}\mathbf{U}^H = \mathbf{I} \quad (21)$$

Where  $\mathbf{U}$ ,  $\mathbf{V}$  are unitary, meaning (20), and  $\mathbf{\Lambda}$  contains the singular values of  $\mathbf{H}$  on its diagonal.

The precoding is done by multiplying  $\mathbf{V}$  with the outgoing waveforms (22) before transmission and  $\mathbf{U}^H$  with the received waveforms (23).

$$\mathbf{x} = \mathbf{V}\mathbf{s} \quad (22)$$

$$\mathbf{r} = \mathbf{H}\mathbf{x} = \mathbf{H}\mathbf{V}\mathbf{s} = \mathbf{U}\mathbf{\Lambda}\mathbf{V}^H\mathbf{V}\mathbf{s} = \mathbf{U}\mathbf{\Lambda}\mathbf{s} \quad (23)$$

$$\tilde{\mathbf{s}} = \mathbf{U}^H\mathbf{r} = \mathbf{U}^H\mathbf{U}\mathbf{\Lambda}\mathbf{s} = \mathbf{\Lambda}\mathbf{s} \quad (24)$$

Here  $\mathbf{s}$  is the symbol for transmission,  $\mathbf{x}$  is the transmitted symbol and  $\mathbf{r}$  is the received symbol. Going through (22-24) it can be seen that the estimated received symbol  $\tilde{\mathbf{s}}$  is equal to the transmitted symbol times the eigenvalue for its channel.

When using SVD the power transmitted for each channel is equal giving the best channel the highest received signal power. Using clever algorithms this can be used to transmit a higher order constellations where the channel is good and lower order or not at all where the channel is bad, this is not done here and a fixed constellation is used across all channels for a fixed bit rate.

A variation of the SVD is done with inverse power allocation matrix  $\mathbf{P}$  which is computed as

$$\mathbf{P} = \mu\mathbf{\Lambda}^{-1} \quad (25)$$

$$\mu = \sqrt{N_t / \text{tr}(\mathbf{\Lambda}^{-2})} \quad (26)$$

Here  $\mu$  is a scaling constant to make sure power is constant,  $N_t$  is the number of transmit antennas and  $\text{tr}()$  is the trace of the  $\mathbf{\Lambda}^{-2}$  matrix. The precoding then takes the form of

$$\mathbf{x} = \mathbf{V}\mathbf{P}\mathbf{s} \quad (27)$$

$$\tilde{\mathbf{s}} = \mathbf{\Lambda}\mathbf{P}\mathbf{s} = \mu\mathbf{s} \quad (28)$$

Here the power is distributed in inverse of the strength of the channels, giving the weakest channel more power than the strongest and equalizing the received power so all bit streams see the same received power.

## 2.7 Theoretical throughput

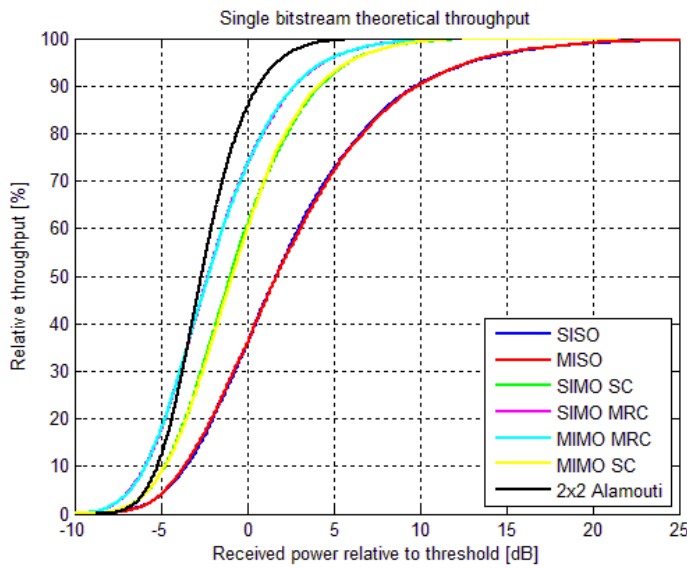


Fig. 1 Comparison of single bit stream throughputs relative to 0dB threshold for the 1x1, 1x2, 2x1 and 2x2 system

Figure 1 shows the theoretical throughput for single bit stream over the RIMP channel for the combining methods used in this thesis. Here it can be seen clearly that adding a second antenna without any form of pre-coding does not provide any gain to throughput. The SISO and MISO are overlapping and SIMO and MIMO overlap as well but MIMO with Alamouti pre-coding provides full transmitter and receiver diversity gain. This overlap happens due to no additional power or diversity being added to the system with additional transmit antennas when an identical data stream is transmitted on both antennas.

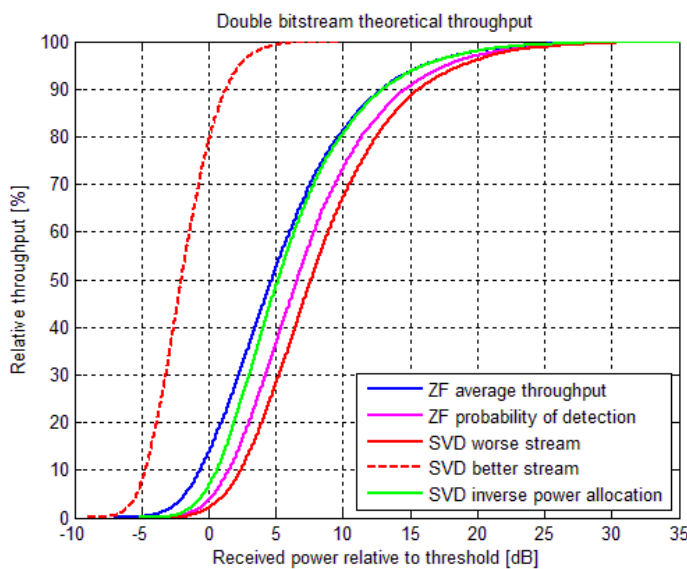


Fig. 2 Comparison of double bit stream throughputs and probabilities of detection relative to 0dB threshold

Figure 2 shows the theoretical throughput for the double bit stream methods used over the RIMP for the implemented methods. Zero forcing and SVD with inverse power allocation both bit-streams have the same received power per bit stream while the SVD has two clearly separate bit streams in terms of performance.

Comparing the worst case bit streams gives the probability of detection (POD), for that purpose the minimum instantaneous throughput for ZF is plotted so that POD of all three methods can be compared.

## 2.8 Total isotropic sensitivity

According to [4] total isotropic sensitivity (TIS) has a simple theoretical relationship with throughput based on the threshold receiver model. It is also stated there that the TIS is equal to the threshold power or

$$P_{TIS} = P_t / e_{rad} \quad (29)$$

Where  $e_{rad}$  is the antenna radiation efficiency of the DUT. In order to verify that the threshold was chosen at 2% packet error and with a large enough amount of samples then (30) becomes valid.

$$P_{TIS} = 1 / \left( \frac{1}{N} \times \sum_{k=1}^N 1/P_k \right) \quad (30)$$

Here  $P_k$  is the power level at which the k-th stirrer position that gives 2% block error rate.

Alternatively TIS can be approximated according to [4] and [18] at 36% throughput for the SISO OTA case

## 2.9 Total radiated power

Knowing the total radiated power of a device can be important for some devices such as mobile phones and other handheld wireless devices to ensure that the device isn't radiating power beyond what can be harmful for the user. The method specified in [15] for measuring the total radiated power (TRP) or total communication power (TCP) of cellphones was used for the basis of the measurement procedure in this work.

$$TCP = \frac{1}{N} \sum_{i=1}^N \frac{1}{3} \left[ \frac{P_{avA}(f_i)}{P_{refA}(f_i)} + \frac{P_{avB}(f_i)}{P_{refB}(f_i)} + \frac{P_{avC}(f_i)}{P_{refC}(f_i)} \right] \quad (31)$$

Here N denotes the total number of frequency points centered around the carrier frequency  $f_i$  taken and  $P_{avA}$  denotes the average measured power at port A of the reverberation chamber and  $P_{refA}$  denotes the reference power lost over the cables and fixed antennas of the reverberation chamber leading to port A. Subscripts B and C denote ports B and C.

For the measurements performed here each frequency band over the operational band of the USRP was measured separately at 50MHz intervals to gain insight into the power radiated by the USRP at each frequency so the frequency averaging in (31) was skipped as only single frequency points were investigated. Since traditionally when measuring TRP of a device the device antenna is attached and plays a part in the TRP the efficiency of the antenna under test was subtracted from the transmission power of the USRP according to (31)

$$TRP_{ref} = P_{tx} + A_e \quad (31)$$

Here  $P_{tx}$  denotes the transmitted power of the device in dBm and  $A_e$  denotes the antenna efficiency in dB. Knowing the cable and chamber losses the measured TRP can be calculated as (32)

$$TRP_{meas} = P_{rx} - A_{chamber} - A_{cables} \quad (32)$$

Here  $P_{rx}$  denotes the received power in dBm,  $A_{chamber}$  denotes the losses in the chamber in dB including the fixed wall antennas and  $A_{cables}$  denotes the cable losses in dB

## 2.10 Radiation efficiency

It has been shown in [16] that the reverberation chamber can be used to measure the radiation efficiency of antennas according to

$$e_{AUT} = \frac{T_{AUT}}{T_{ref}} e_{ref} (1 - |S_{11}|^2) \quad (33)$$

Here  $e_{AUT}$  denotes the efficiency of the antenna under test (AUT) and  $T_{AUT}$  the total transfer function of the antenna under test.  $T_{ref}$  and  $e_{ref}$  denote the reference antennas transfer function and efficiency respectively and  $S_{11}$  is the reflection coefficient of the AUT. This poses a limitation to the measurement using the USRP as the USRP cannot measure the complete S parameters of the system, only the  $S_{21}$  or transfer function. Thus if the reflection coefficient of AUT is not very small the efficiency of the antenna cannot be measured accurately without knowing it beforehand.

## 2.11 Doppler spread

It is well known that when there are moving scatterers, or either the transmitter or receiver is moving there will be Doppler shift introduced according to

$$f = \left( \frac{c+v_r}{c+v_s} \right) f_0 \quad (34)$$

Here  $f$  denotes the observed frequency,  $f_0$  denotes the transmitted frequency,  $c$  is the propagation velocity and  $v_r$  and  $v_s$  denote the velocity of the receiver and source. When many such components are introduced to a single tap the difference between the shifts is known as the Doppler spread of the channel. Knowing the Doppler spread gives an indication of the quality of channel and can be used to calculate the coherence time of the channel. In [17] it has been shown that the Doppler spread in the reverberation can be predicted from stationary measurements using arbitrary time between each step to calculate the rotation speed of the stirrers. If the channel transfer function is denoted as  $h(f,t)$  in frequency and time, it is complex and its autocorrelation function,  $R_h(f,\partial t)$  is complex conjugate symmetric then the Doppler spectrum can be defined as

$$D(f, \rho) = F\{R_h(f, \partial t), \partial t\} \quad (35)$$

Knowing that the autocorrelation function can be alternatively defined as

$$R_h(f, \partial t) = h(f, \partial t) * h(f, -\partial t) \quad (36)$$

Where  $*$  denotes convolution. Applying the Fourier transfer  $F\{ \}$  to  $h(f,t)$  then the Doppler spectrum can be alternatively defined as

$$D(f, \rho) = H(f, \rho)H^*(f, \rho) = |H(f, \rho)|^2 \quad (37)$$

This can be easily computed from knowing the step wise transfer functions of the reverberation chamber having  $\Delta t$  between them which is defined as

$$\Delta t = T/N \quad (38)$$

Where  $T$  is the total revolution time and  $N$  is the number of samples and the maximum Doppler frequency  $\rho$  will be

$$\rho_{max} = \frac{1}{2\Delta t} \quad (39)$$

## 2.12 Delay spread

In a rich multipath environment there will be multiple reflections of an incident wave and where the paths are different in length there will be a delay between the arrival times of the waves. Knowing the delay spread can give an idea of the channel richness and give an indication if there will be inter symbol interference if the symbol duration is short relative to the delay spread. Here the RMS delay spread is defined in [21] as

$$\sigma_\tau = \sqrt{\tau^2 - (\bar{\tau})^2} \quad (40)$$

$$\bar{\tau} = \sum_k P(\tau_k) \tau_k / \sum_k P(\tau_k) \quad (41)$$

$$\tau^2 = \sum_k P(\tau_k) \tau_k^2 / \sum_k P(\tau_k) \quad (42)$$

Here  $\sigma_\tau$  in (40) denotes the RMS delay spread and  $P(\tau)$  is the power measured at time  $\tau$  relative to transmission. The mean excess delay is defined in (41). Here the received powers are relative so calibration of transmitted/received power is unnecessary

### 3 System description

All of the project code is done in LabView with channel simulations done in Matlab. LabView is a graphical coding environment which builds up a control and computation program for the USRPs and digital attenuator (DA). The LabView code, known as virtual instruments (VIs), is used to set all parameters of the system including sampling rate, carrier frequency and modulation. All baseband processing happens at the code level while modulation from baseband to radio frequency and back is done by the USRP hardware.

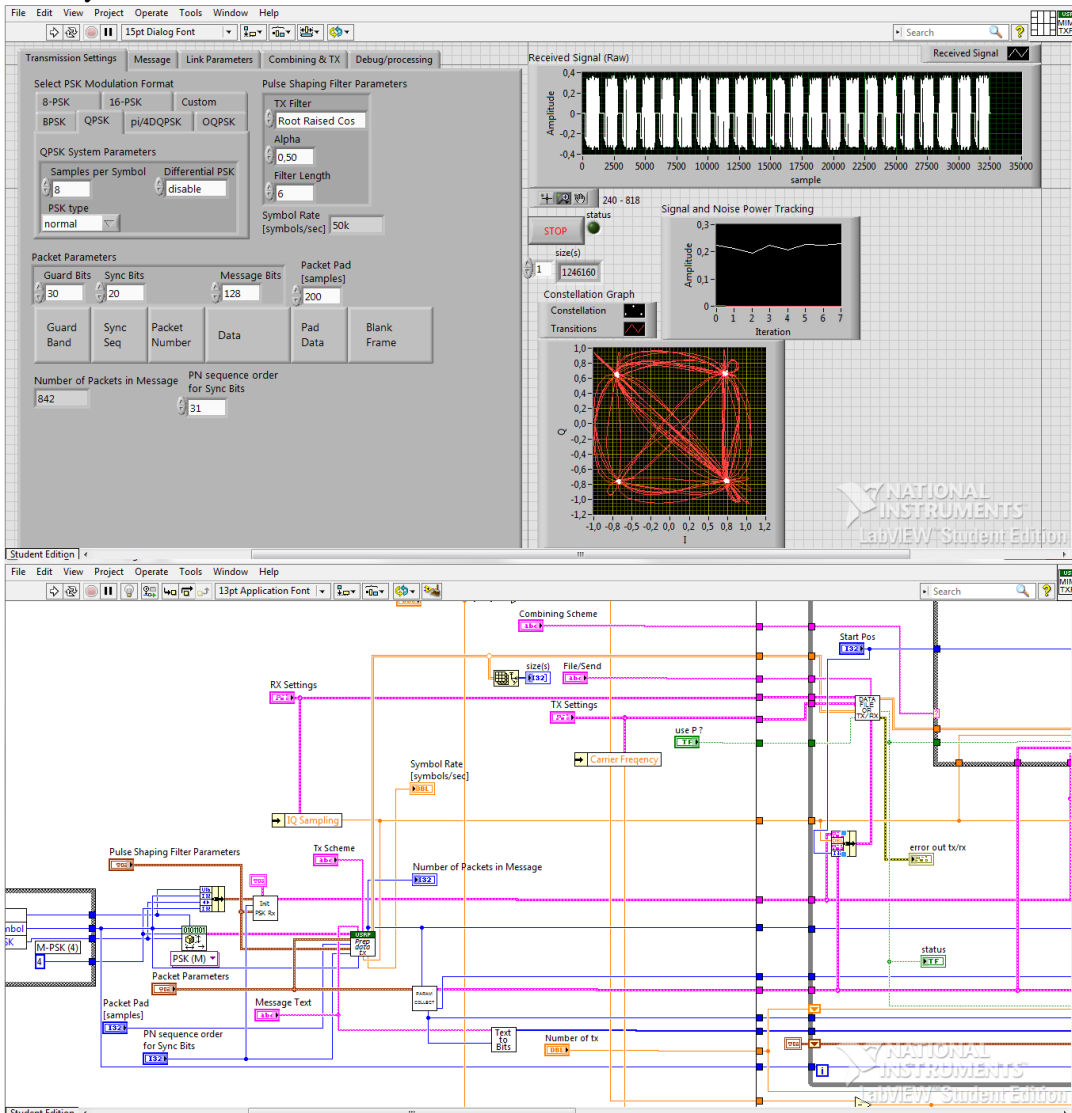


Fig. 3 Preview of the LabView front panel and code used in this project

The code used for this project is based on the examples provided by National Instruments [7], [8] but has been expanded and modified significantly in order to accommodate the needed parameters..

For these measurements the system parameters were chosen so that it was operating at a relatively low throughput compared to what can be achieved by the USRP platform. The chosen sampling rate was 400 kHz and each symbol is selected as 8 samples, giving a symbol rate of 50k symbols/sec. This allows for a maximum of 100kb/s bit rate using gray coded quadrature phase shift keying (QPSK) but due to a large packet overhead (Fig. 3) which was maintained from the initial example the code is based on the achieved bitrate was only 33kb/s.

For the operating frequency 915MHz and 1800MHz were chosen as center frequency, with a root raised cosine as the pulse shaping filter with a roll off factor of  $\alpha=0.5$  and length of 6 symbols, the

system bandwidth is 75kHz ( $B_{\text{system}}$ ). Given that during transmission the coherence bandwidth of the chamber ( $B_{\text{coherence}}$ ) was 3.5MHz the channel was flat fading as  $B_{\text{system}} \ll B_{\text{coherence}}$ . Care was taken to make sure the antennas were uncorrelated inside the chamber as can be seen in figure 5.

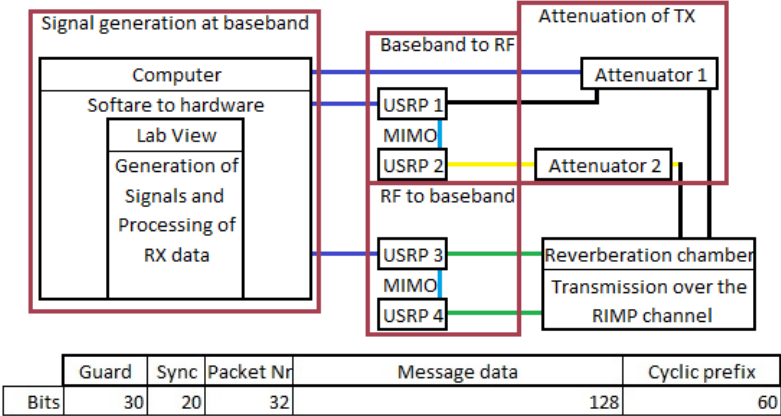
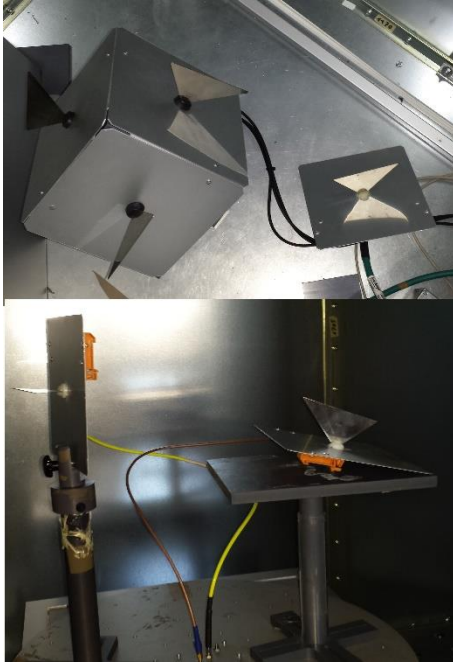


Fig. 4 Block diagram of the measurement setup and distribution of bits in packet

Figure 4 top portion shows the general block diagram of the measurement setup for throughput measurements for the 2x2 system. For other measurements the number of USRPs and/or attenuators used was reduced but the general system layout remained the same. In the bottom portion the packet build up can be seen with relative length per each component.

During over the air (OTA) for the single bit stream measurements the measuring was done in 1dB increments over a range from -50dBm to -90dBm of received power, at 915 MHz a total of 33.380 packets split into 842 packet messages which were sent 40 times at each attenuation with the RC in continuous operation. At 1800 MHz half that was transmitted or 16.840 packets in 20 messages of 842 packets, the number of packets sent at 1800 MHz was reduced due to time constraints. For the double bit stream cases the measurements were performed over the range of -60dBm to -90dBm received power with 200 packets sent at each stirrer position with the chamber being stepped through 300 stirrer positions for a total of 60.000 packets or 30.000 packets per bit stream.



*Fig. 5 Antenna placement inside the reverberation chamber*

Fig. 5 shows the antenna placement for the throughput measurements inside the RC. Top picture shows the transmitting antennas and bottom picture shows the receiving antennas on the rotating plate. For measurements only one of the static antennas provided by the chamber is active at a time.

### 3.1 Detailed description

This chapter will seek to provide some insight into the more detailed operation of the throughput code used for this project

#### 3.1.1 Packet transmitter

The packet transmitter is based on the example provided by [1]. The core functionality of it has not been changed. A random ASCII text is chosen as the message for transmission and decoded into binary format and the binary padded so that the total number of bits to be transmitted matches the total number of bits per packet times the number of packets. Each packet has the same user defined construct, guard period of empty samples, guard period of binary bits, synchronization bits, packet number, data packet and cyclic bits. All these values can be user defined except the packet number and cyclic bits.

- The guard period of empty samples provides no gain over the guard bits except easy visual identification of individual packets making for simpler debugging. Excessively long guard periods should be avoided in order to reduce throughput degradation.
- The guard bits provide a period of maximum received power allowing for more accurate frame detection, excessively long guard periods should be avoided but too short provide for poorer performance on frame detection.
- The synchronization bits are a pseudo random bit sequence that is known both by the transmitter and receiver. This allows for phase correction at the receiver side and preliminary packet detection.
- The packet number is a 32 bit representation of the number of the packet so that data order can be maintained at the receiver side.

- The length of the data packet relative to the length of the overhead defines the absolute throughput of the system. If absolute throughput is of concern this number should be maximized for the channel coherence time.
- The cyclic bits are appended in order to provide padding for internal LV filters when modulating and demodulating.

Once the packets have been constructed they are translated to symbols which are QPSK gray coded in this application and the symbol filter applied so the waveform is ready for transmission

For cases where full channel state information is required at the receiver side an extra pair of synchronization bits are added and made non-overlapping to each other. That way the receiver can see the individual synchronization sequence from each transmitter

### 3.1.2 Packet receiver

The packet receiver is based on the example provided by [1] with modified functionality to allow for combining at the receiver side. Where there is no combining performed the received waveform is broken down into manageable chunks and fed into the demodulator. The demodulator has inbuilt functionality to perform phase correction as long as all the packets in each chunk are close to each other in phase.

If there is to be any combination or algorithms to be applied to the received waveforms, i.e. MRC or SC, they are applied directly after reception before the demodulator.

After the demodulation the received bit stream is partitioned down into packet chunks and checked for validity. The initial test is if the synchronization sequence is correct, if it is correct then the packet number is checked to see if it corresponds to a number that has been sent. If the number is within the sent range the binary is stored and compared against the initial transmitted binary and if there is a 90% match the packet is accepted as correct.

Once all packets have been checked for validity they are decoded back to text with zero padding for the missing packets.

### 3.1.3 Transmitter and receiver

The initial examples provided by [1] are stand alone and the receiver and transmitter are completely asynchronous. For ease of testing a semi synchronous transceiver was implemented. If the number of USRPs being used is two or less then they can be completely synchronous and is the preferred method as that avoids any frame detection issues. If the number of USRPs exceeds two then the transmitted data needs to be padded with silence to allow for non-synchronous start of the transmitter and receiver pairs.

For accurate testing transmitters and receivers must be synchronized so receivers are synchronous with each other and transmitters likewise, this can be readily done with the supplied code as the USRP can accept external synchronization signals both over a proprietary cable or external clock.

In this application the whole data set to be transmitted is fed to the transmitter which is started in a semi fixed time relative to the receiver. The offset between them is in the order of 2-5ms and can be compensated for by setting the start times properly.

The exception from the continuous transmission and reception of the data in a single chunk is when pre-coding is required, then a pilot signal is transmitted on a separate transmission, processed for the pre-coding and the pre-coded message finally transmitted over the semi synchronous transmitter.

## 3.2 Limitations

While the USRP is a viable platform for many forms of testing it is limited by the network speed, sampling rate (20MHz -40MHz) and processing power of the control computer which it is dependent upon. For simple systems that do not rely on CSI at the transmitter side it can measure throughput quickly and accurately as will be shown in the results.

When the system needs CSI at the transmitter side the system becomes limited by the initialization time of the USRP which is fairly high (120ms) meaning that the channel must be practically stationary or the preceding channel estimate will become invalid for the pre-coding.

A further limitation when CSI at the transmitter side is required is that the channel measured by the USRP is uniformly distributed in phase even when it is stationary. That is when two measurements are performed that are separated in time and the devices are de-initialized between the measurements the measured channel does not have the same phase. This is due to the phase locked loop locking at random times causing the perceived channel to be random. This can be worked around by having both transmitter and receiver synchronize to an external 10 MHz reference frequency and implementing continuous transmission and reception from training sequence to data if CSI is required at the transmitter side.

Processing for larger algorithms should be done offline unless the control computer has a high processing capacity or the algorithms heavily optimized in order to avoid excessive wait time between transmissions. Offline processing is easy to implement if sufficient memory is available so this is not an obstacle.

The hardware itself also suffers limitations due to significant crosstalk between the transmitter and receiver channels, meaning that for low received power measurements separate USRPs must be used as TX and RX. The receiver threshold appears to be heavily influenced by the driver version so care must be taken to maintain the version and re measure the threshold if updates are done.

## 4 Measurement setup & results

In the following chapters a more detailed description of the measurement setup for each procedure and its results will be discussed

### 4.1 Throughput measurements

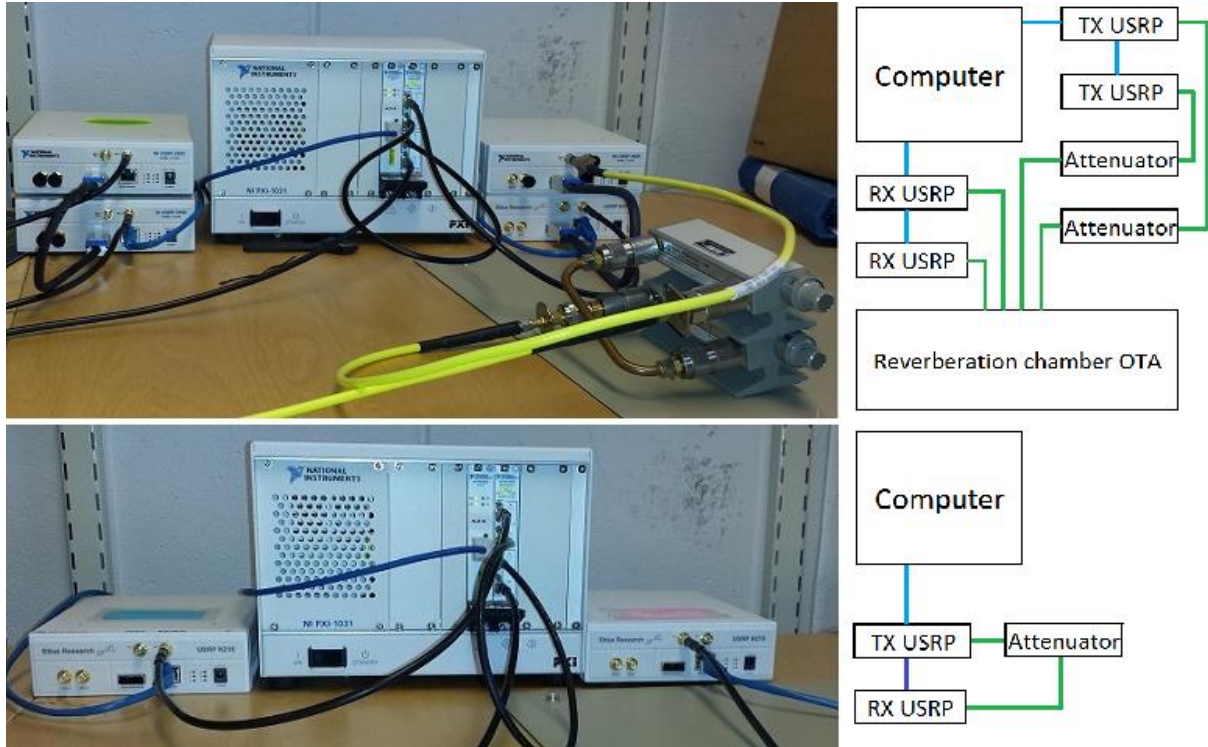


Fig. 6 Conductive and OTA measurement setup

Fig. 6 shows the setup of the USRPs used for measuring the throughput at 915MHz and 1800MHz, both OTA (top) and conductive (bottom).

For all of the single bit stream OTA measurements except the Alamouti algorithm the reverberation chamber was run continuously so that the observed channel was random at each instant. For the double bit stream and Alamouti algorithm the chamber was stepped through 300 stirrer positions for a message wise static channel but overall random for the total transmitted data. This was done to overcome the timing limitation of pre-coding for SVD.

Overall it can be seen in the following figures 7-16 that the agreement between measured and theoretical throughput follows closely or within 1,5dB for most points measured where implementation was successful. This is due to 0,5dB standard deviation inside the RC and 1dB standard deviation from the USRP when measured over 40 points. There is a slightly larger standard deviation between the theoretical and measured at 1800 MHz than at 915 MHz and that is due to the halved number of total packets transmitted.

### 4.1.1 Single input, single output (SISO)

The SISO measurement setup was the most used setup for measurements as most system and channel parameters were also measured using the same setup with slight variations. For throughput two setups were used.

First the conductive setup where two USRPs were connected with a single network cable to the control computer and their clock was synched over the MIMO cable. The transmitting USRP was then connected to an attenuator and then from the attenuator to the receiving USRP. The attenuator was stepped down until there was no throughput of data. The results of which can be seen in figure 7. This was also repeated for higher sampling frequencies but with fixed samples per symbol at 800 kHz and 1.2 MHz at 915MHz center frequency and the absolute throughput compared as can be seen in Fig. 8

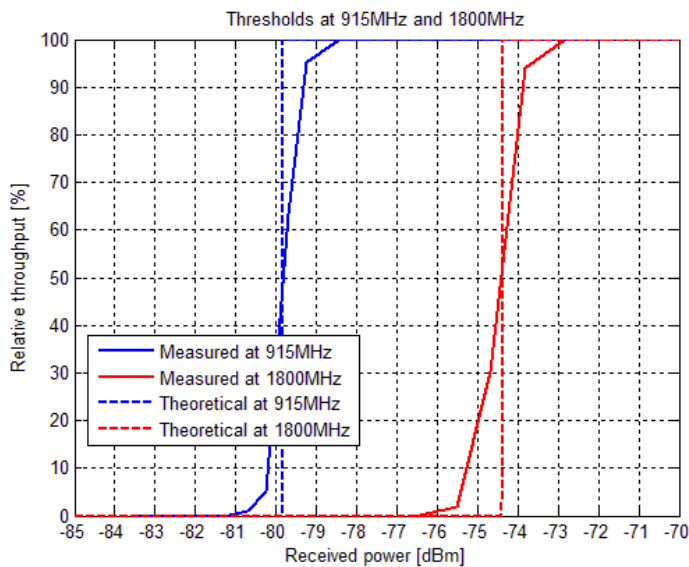


Fig. 7 Conductive measurements of the SISO system

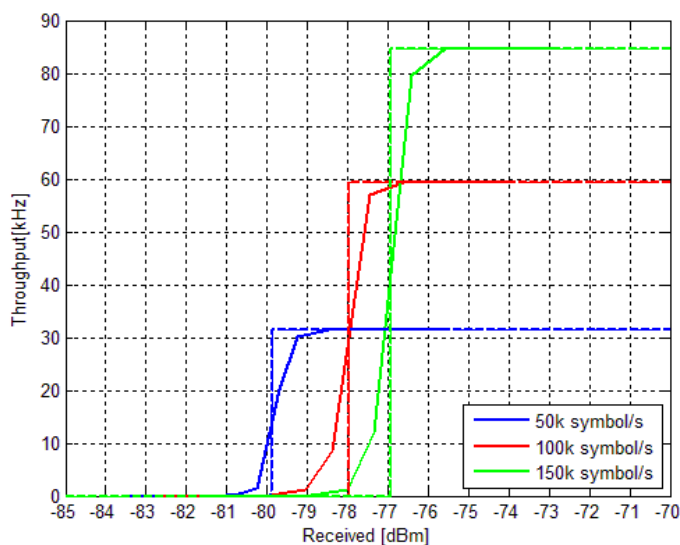


Fig. 8 Absolute throughput for various sampling frequencies with solid lines measured data and dashed lines theoretical values

Figure 8 Shows how the absolute throughput compares as the sampling frequency is improved. This is done with the same packet buildup as other OTA testing so it is far from the theoretical maximum throughput of 300kb/s at 150k symbols/s. Even though the symbol rate is tripled at 150k symbols/s compared to 50k symbols/s the throughput does not triple as the initialization overhead remains static but grows in relation to the message length in time.

For the OTA measurements the setup remained unchanged from the conductive setup except that instead of connecting from the attenuator to the receiving USRP directly the attenuator output was connected to the RC whose output was connected to the receiving USRP.

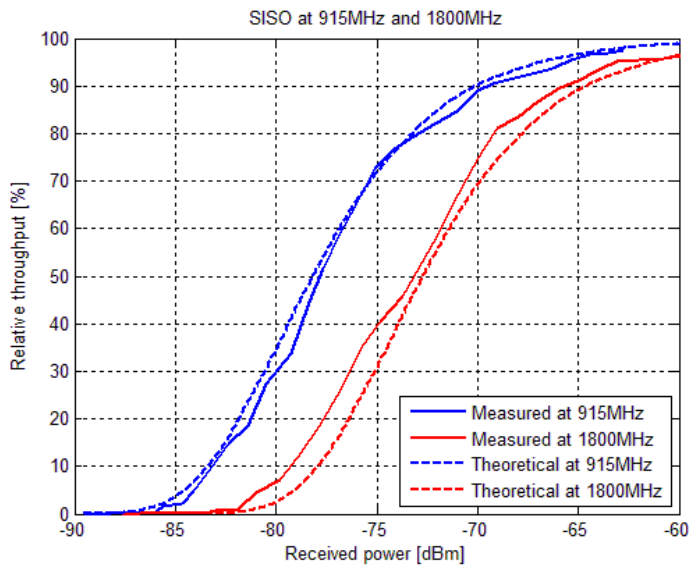


Fig. 9 OTA measurements of the SISO system

Figure 9 shows the results of the OTA measurements for the SISO system. This was also repeated for the same sampling frequencies as the conductive at 915MHz center frequency and the absolute throughput compared

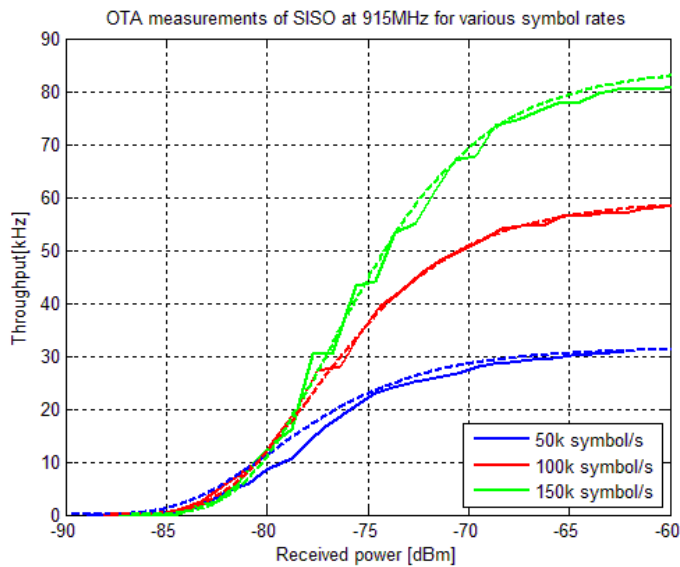


Fig. 10 Absolute throughput of different symbol rates OTA with solid lines measured data and dashed lines theoretical values

Figure 10 shows a very good agreement between the predicted throughput accounting for overhead and the measured values.

As can be seen in figures 7-10 there is a very good agreement between the measured values and the simulated theoretical values for all configurations for the SISO bit stream setup.

### 4.1.2 Multiple input, single output (MISO)

For the MISO setup the same setup was used as for the SISO but a 3dB splitter was applied after the attenuator and both of its outputs connected to the reverberation chamber, which has a total of 3 active antennas inside now.

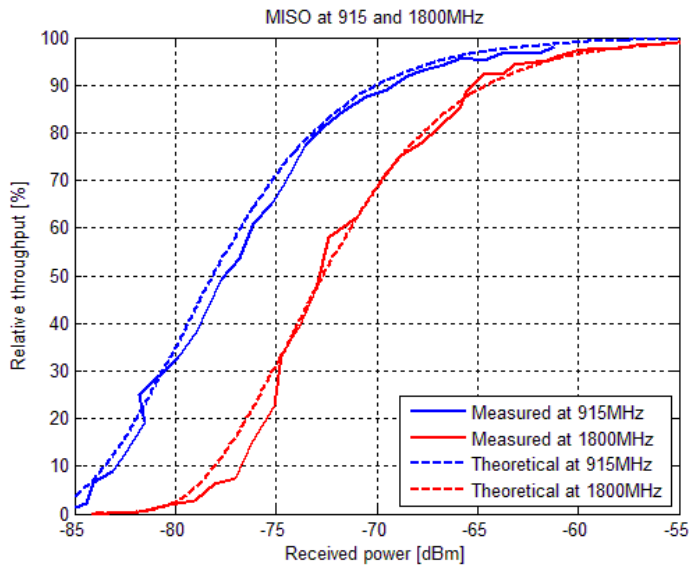


Fig. 11 OTA results of MISO throughput measurements

Figure 11 shows an overall good agreement between measured and theoretical values at 915MHz but the system performance degrades faster than anticipated at 1800MHz this can be explained by the reduced number of total packets sent resulting in a number of packets received at lower power being statistically insignificant.

### 4.1.3 Single input, multiple output (SIMO)

The setup for the SIMO measurements was so that the transmitting USRP was connected to the attenuator and the attenuator to the reverberation chamber input and the two receiving USRPs were synchronized with the MIMO cable and connected to the reverberation chamber output.

The start of the USRPs that are not synchronized is offset by approximately 50ms and has a variance of +/- 5ms so a sufficiently large wait time was appended to the end and start of each transmission to make sure no data was lost due to lack of synchronization.

It is worth noting that system performance was notably degraded when selection combining was performed on a sample by sample basis so it was extended to operate on a packet by packet basis which provides performance very close to expected theoretical values.

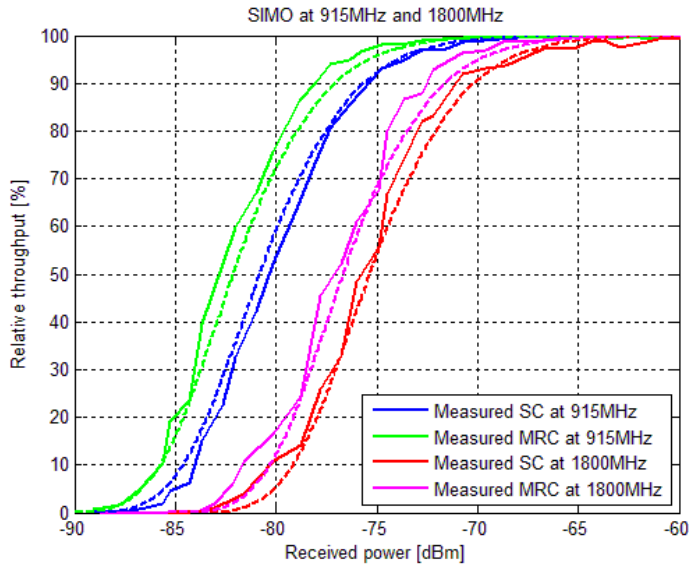


Fig. 12 OTA measurements of SIMO Selection and Maximum Ratio Combining with solid lines measured data and dashed lines theoretical values

Figure 12 shows that the measured and theoretical results for both SC and MRC at 915 MHz and 1800 MHz are in close agreement with each other. The deviations from the expected value at 1800 MHz is due to the smaller amount of packets being transmitted increasing the deviance from the theoretical values

#### 4.1.4 Multiple input, multiple output (MIMO)

For the MIMO system the MISO system was expanded to have a second transmitter that was synchronized with the other transmitter over the MIMO cable and its output connected to a second attenuator and finally to the reverberation chamber for a total of 4 active antennas. The preceding start offset is still in the same range so the same wait time was used.

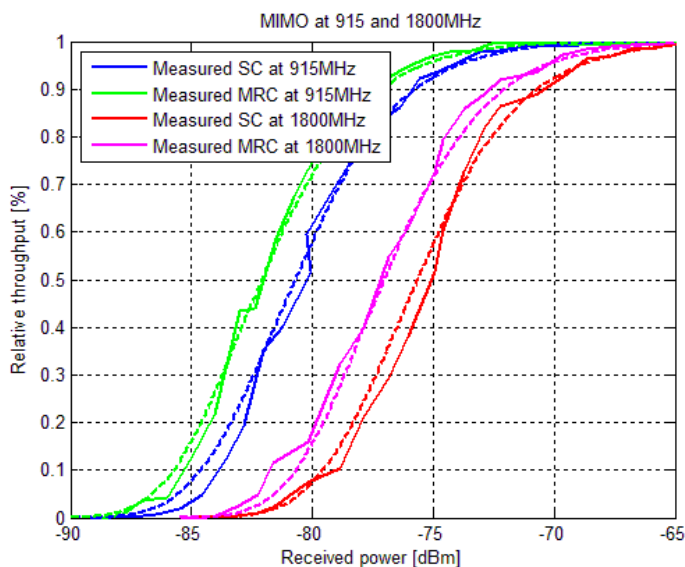


Fig. 13 MIMO OTA measurements for single bit stream with solid lines measured data and dashed lines theoretical values

As can be seen in figure 13 the agreement between theoretical and measured values for the 2x2 MIMO is very good.

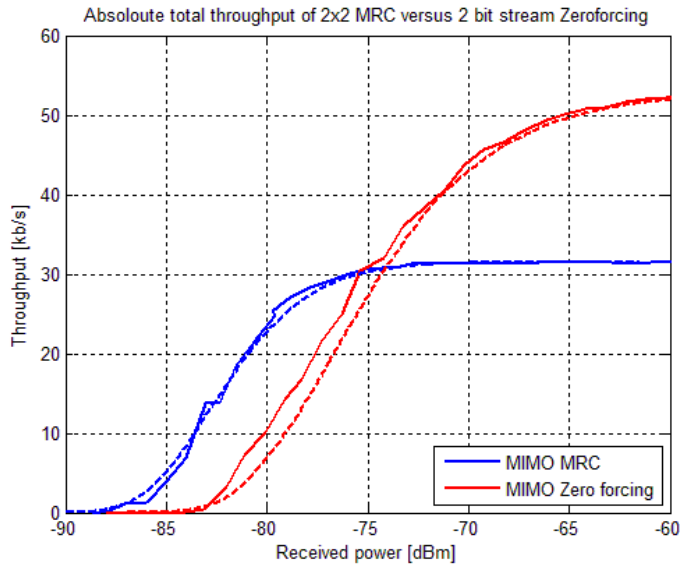


Fig. 14 Absolute total throughput of single bit stream MIMO and combined double bit stream MIMO with ZF with solid lines measured data and dashed lines theoretical values

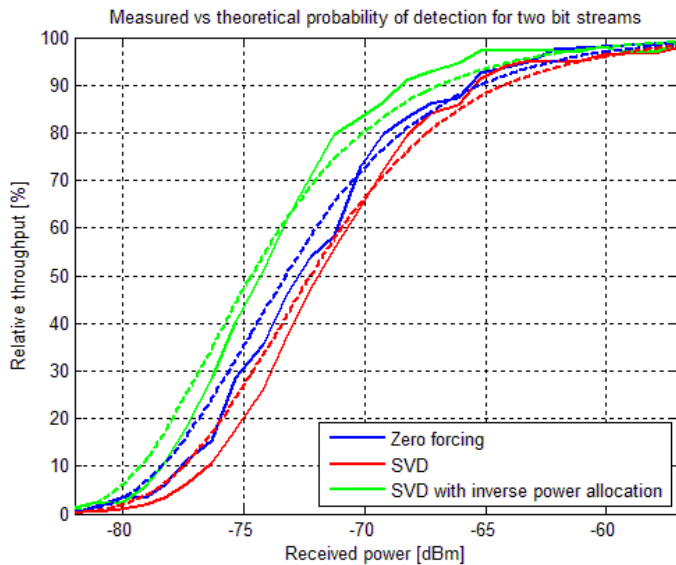


Fig. 15 Measured probability of detecting both bit streams for the two bit stream system with solid lines measured data and dashed lines theoretical values

Figure 14 shows very good agreement with the theoretical throughput for both one and two bit streams using MRC and ZF respectively.

Figure 15 shows the measured probability of detection for both bit streams for the measured two bit stream cases and overall the agreement is good between the theoretical values and measured values. The offset here is most likely due to improper channel estimation as the signal strength decreases making proper frame detection harder and increasing offset from the ideal frame causing the estimated channel to vary more.

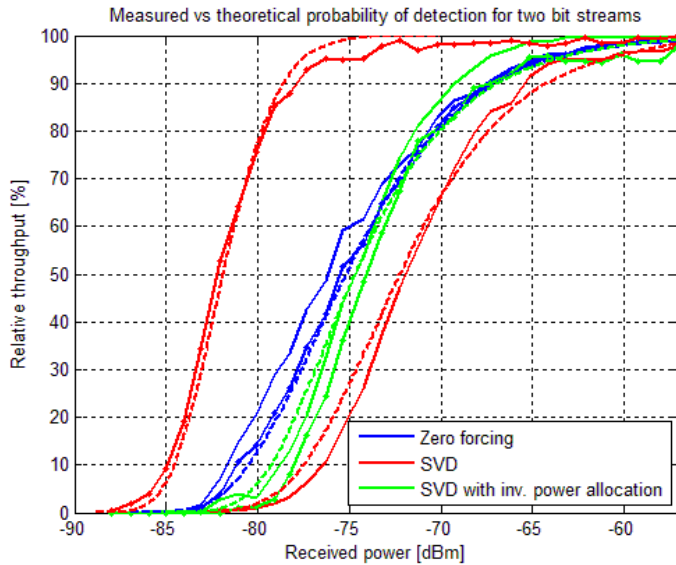


Fig. 16 Measured throughput for individual bit streams of the two bit stream system, here solid lines are measured data and dashed theoretical values

As can be seen in figure 16 the agreement between the theoretical values and the measured for the two bit stream system is overall good. Although theoretically both bit streams for the ZF and SVD with inverse power allocation should be identical there is a slight discrepancy of 1dB between them when measured, this can be allotted to imperfect channel estimation and potentially bad antenna placement inside the reverberation chamber to some degree.

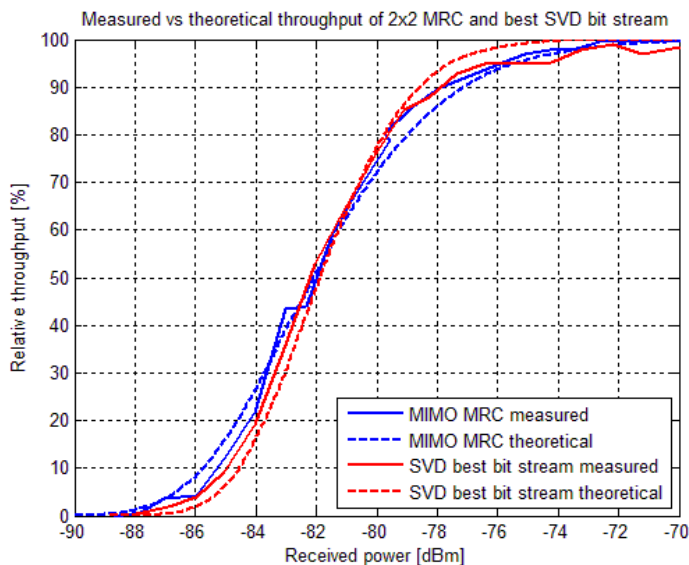


Fig. 17 Throughput of single bit stream 2x2 MIMO MRC vs better bit stream of SVD

As can be seen in figure 17 the measured throughput for single bit stream 2x2 MIMO MRC is near identical to the measured throughput of the better bit stream of the 2x2 SVD indicating that a larger number of samples with improved channel estimation should be used to differentiate between algorithms that perform close to each other theoretically.

For all methods measured for the MIMO system an overall very good agreement can be seen in figures 13-16. The exception to this is the Alamouti algorithm whose implementation was unsuccessful in a timely manner and therefore is not compared here.

## 4.2 System Parameters

In this portion the results of measuring various system properties using the USRP will be presented and discussed. The selected model of USRP has an operating range from 50MHz to 2200MHz which provides the upper limit to all measurements performed over a range of frequencies. The lower limit is supplied by the RC and the reference antenna. The RC model used for measurements does not support enough wave modes below 500MHz and the reference disc cone antenna is not calibrated below 750MHz providing a lower range of interest for measurements.



Fig. 18 Disc cone reference antenna used for calibrations

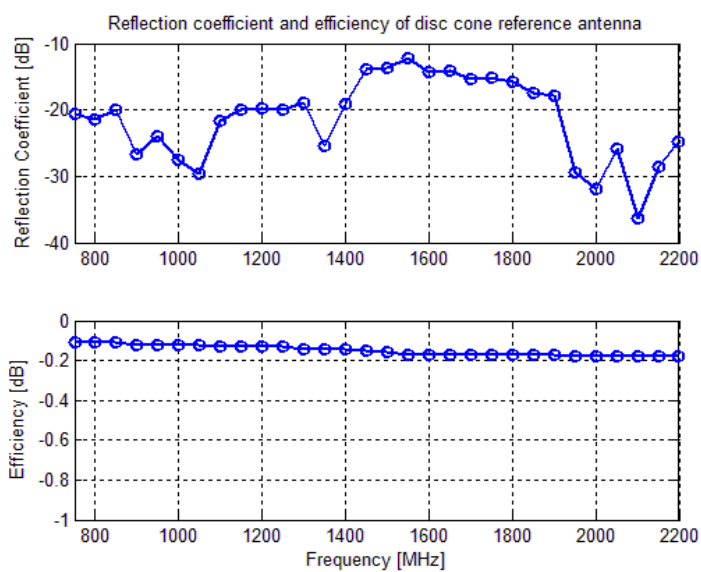


Fig. 19 Reflection coefficient and efficiency of the reference antenna

As can be seen in figure 19 the antenna pictured in figure 18 has a very high efficiency over the entire frequency range of interest and a very low reflection coefficient making it a very good antenna for reference measurements.

#### 4.2.1 NI USRP N210 properties

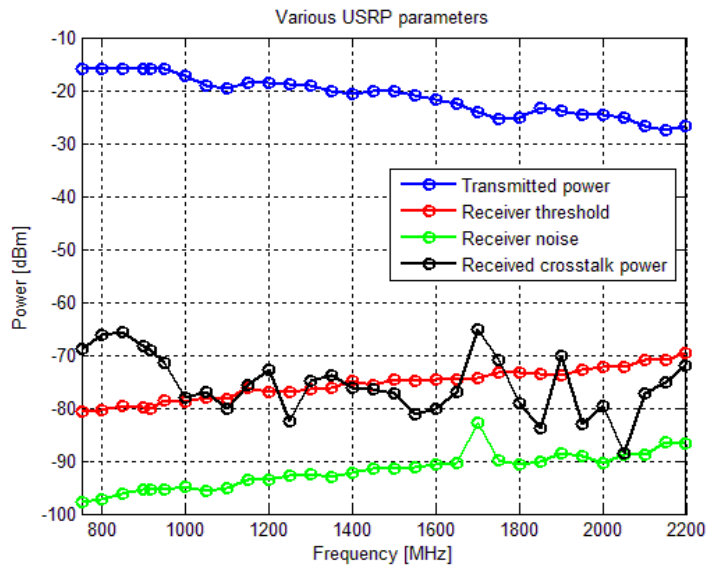


Fig. 20 Various properties of the N210 USRP model used

As can be seen in figure 20 the receiver noise measured with no transmitting USRP and 50Ω load on the receiving ports is below -85dBm for most of most of the operating range. The transmitted power is measured using a 10 kHz sinusoid with maximum amplitude with 0dB TX gain.

A large problem for higher frequency measurements comes with the decreasing sensitivity and reduced transmit power on higher frequencies, this results in significantly less signal strength being received at higher frequencies potentially leading to measurement inaccuracy. A total of 10dB power reduction can be seen both in receiver sensitivity and transmitted power from 750MHz to 2200MHz.

The second limitation of the USRP set up comes from the high power of measured crosstalk. Here the same USRP is set to transmit and receive with both ports terminated in 50Ω loads and the power received measured by the USRP. For many frequencies this power is greater than the receiver sensitivity resulting in crosstalk between transmitter and receiver before being transmitted OTA.

The receiver threshold is measured using the packet transmitter used for the conductive throughput so it will vary with implementations but shows the general trend of the hardware sensitivity as the only variable in those measurements is frequency and transmitted power which has been accounted for.

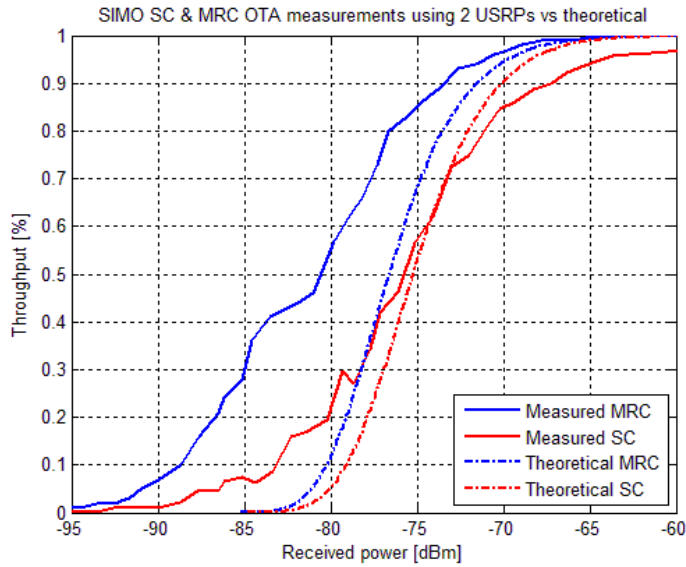


Fig. 21 Effects of crosstalk on SIMO throughput

As can be seen in figure 21 the effects of the crosstalk become severe as the incident power from antennas is reduced rendering the platform useless to low power measurements unless the transmitter and receiver are separate units.

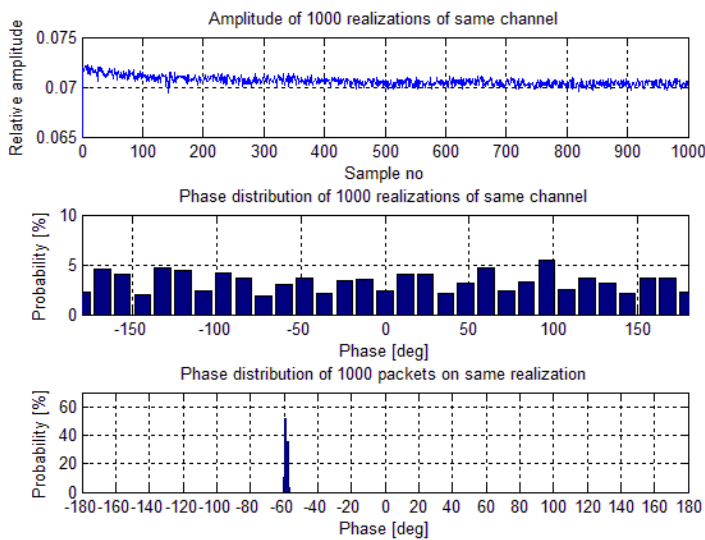


Fig. 22 Amplitude and phase distribution of channel estimation, first phase for individual realizations, second single realization

As can be seen in figure 22 the measured amplitude of the conductive channel is static except for the initial 150 samples as it drops slightly, this is due to the device warming up and highlights the need for having the device warmed before measurements start. In the center subplot the phase for 1000 individual realizations can be seen and is nearly uniformly distributed over the same static conductive channel. The final subplot shows the estimated phase of the packets of a single continuous message over the conductive channel with two frequency synchronized USRPs has a measured phase close to constant or standard deviation of 0.62 degrees.

This random phase has no effect on throughput where there is no pre-coding as the phase can be estimated on a packet by packet basis but makes pre-coding challenging as the channel estimation and

transmission of the pre-coded data has to be done on the same initialization of the transmitter and receiver. Furthermore it is important that the transmitter and receiver are frequency synchronous for the phase to remain fixed in time should pre-coding be required.

### 4.2.2 Total isotropic sensitivity (TIS)

For measuring the total isotropic sensitivity a high efficiency disc cone antenna (figure 18) was used on the receiving side of the reverberation chamber and the transmitting and receiving USRPs were put on a synchronized clock to minimize potential errors due to improper frame detection. The transmitting USRP connected to the input of the digital attenuator, whose output was connected to the RC input and the RC output to the receiving USRP.

The chamber was then stepped when the 2% PER level was found at that position. This was repeated for 150 chamber positions. For the estimation of the TIS the 36% throughput level was found with the chamber running continuously. It has been established in [4] and [18] that this level corresponds to the TIS of the device for the SISO system. For reference the measured threshold of the device was compared as threshold level is closely related to TIS.

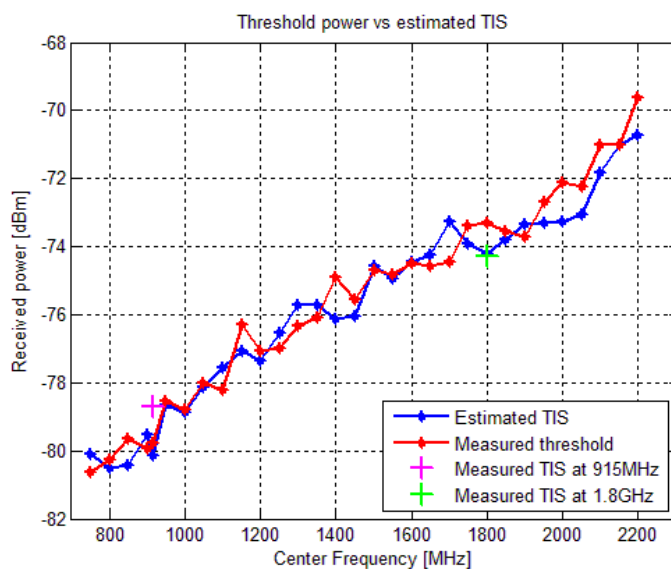


Fig. 23 Measured and estimated TIS of USRP

As can be seen in figure 23 there is a close agreement between the measured TIS, the estimated TIS and the threshold value of the device for the entire frequency range. Here the maximum error over all frequencies 1.2dB is and the mean error over all frequencies is 0.44dB which is very good considering the 0.5dB standard deviation of the RC and 1dB standard deviation of the USRP

### 4.2.3 Total radiated power (TRP)

The measurement setup for TRP was the same as for TIS except that the attenuator was removed from the setup. The chamber was then run and samples gathered 3 second segments for a total of 150 seconds of sampling time at each frequency point.

Reference measurement of the TRP was performed by measuring the device transmitted power with a power spectrum analyzer (PSA) and the antenna efficiency added to the measured transmitted power to calculate the total radiated power.

For measuring the TRP with the USRP the received power was measured as a power average and the losses in the cables, chamber and fixed antennas subtracted from the received power to calculate the TRP

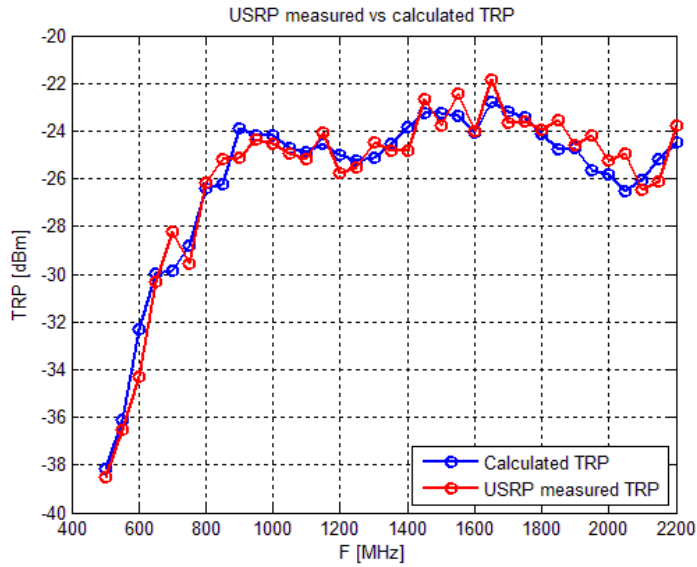


Fig. 24 Measured vs calculated TRP of USRP

Figure 24 shows good agreement between the TRP measured by the USRP and the TRP calculated from the transmitted power and antenna efficiency. The maximum error over all frequencies is 2dB and standard deviation over all frequencies is 1dB making the measurement fairly reliable considering the standard deviation of the RC is 0.5dB

#### 4.2.4 Efficiency

For efficiency measurements the transmitting and receiving USRPs were synchronized over the MIMO cable. The transmitting USRP was connected to a fixed attenuator whose output was connected to the reverberation chamber and the reverberation chamber output connected to the receiving USRP. The USRP internal transmit gain was stepped through a 5dB range and the throughput measured at each point both with the reference antenna and antenna under test as the receiving antenna. In both cases the other antenna was inside the chamber terminated into a 50Ω load to maintain static chamber loading. The antenna under test here was one of the triangle antennas in figure 5.

The measured throughput points were then fitted to a theoretical SISO throughput curve in relative received power and the difference between the reference antenna and antenna under test at the same transmitted power level on the same curve calculated. Finally the difference between all five transmit power pairs was averaged to calculate the efficiency.

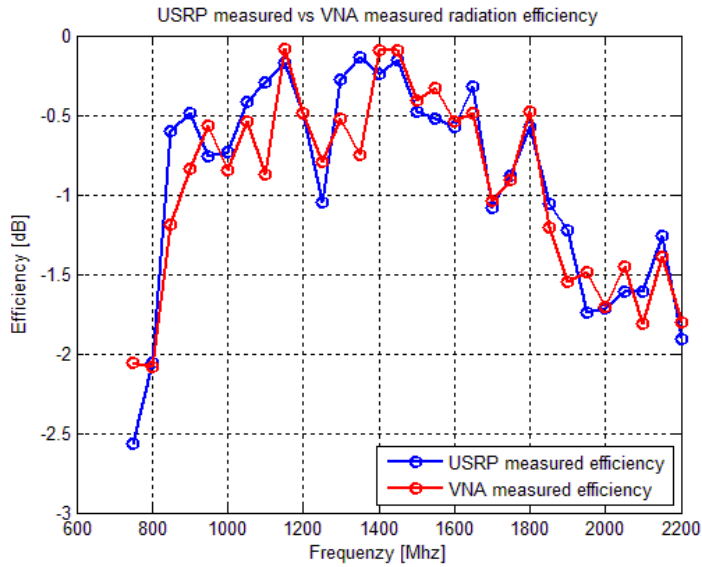


Fig. 25 Total radiation efficiency measured by USRP and VNA

Figure 25 shows the results of the measurements by the USRP compared to the VNA measured efficiency. Overall the curve shows good agreement and maximum over all frequencies 0.6dB offset from the VNA measured efficiency. The use of USRP for efficiency measurements using this throughput comparison method shows relatively good agreement with VNA measured radiation efficiency and provides good reliability as the standard deviation of measurements is 0.3dB

#### 4.2.5 Diversity gain & correlation

For measuring the diversity gain a 10 kHz sinusoid was transmitted on both in- and quadrature-phase and the received power was sorted into 0.1dB bins for a total of 12M samples sampled at 200 kHz at each center frequency and ordered in order to construct the CDF of each individual frequency.

This process was first done with the reference antenna in figure 18 and both of the triangle antennas inside the RC terminated in 50Ω loads using a single USRP pair with the receiver and transmitter synchronized. It was then repeated with both of the triangle antennas in the horizontal configuration with 175mm from center to center and the reference antenna terminated in a 50Ω load.

This was done with the receivers synchronized over the MIMO link and the transmitter freestanding, care was taken so that samples were only calculated while the transmitted sinusoid was being received.

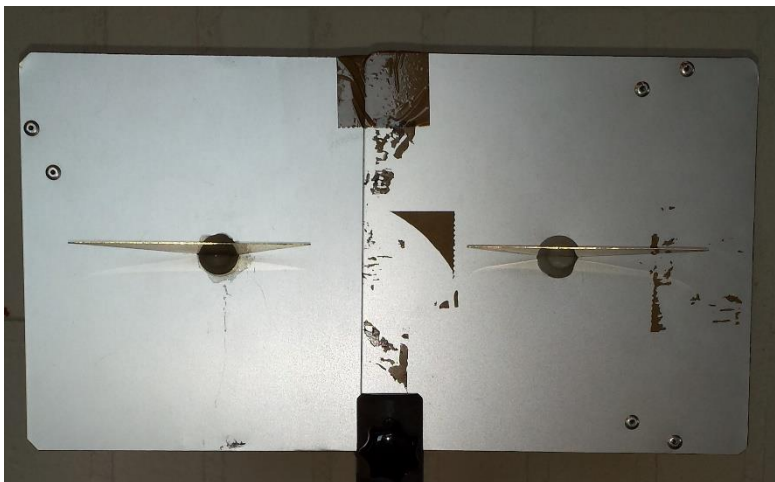


Fig. 26 Horizontal configuration of the triangle antennas

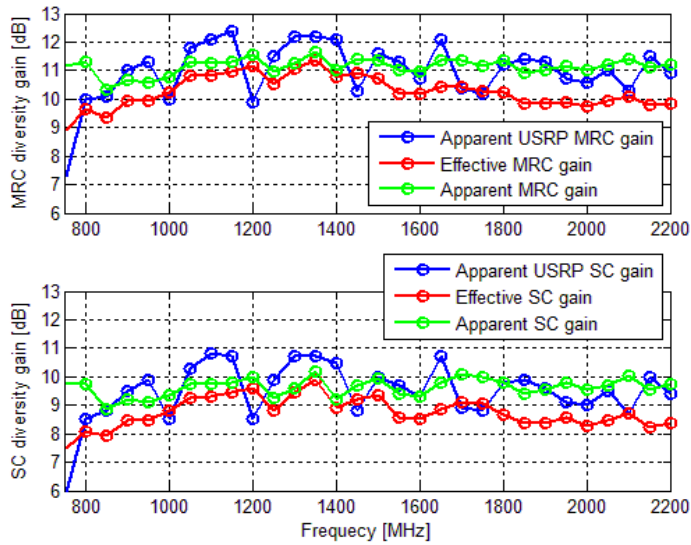


Fig. 27 USRP measured diversity gain vs VNA measured diversity gain

As can be seen in figure 27 the measured diversity gain is of the same order as the reference gain but has a maximum error over all frequencies of 4dB and a mean error over all frequencies of 1dB. This doubled with the fact that measured values exceed theoretical maximums makes the measurements relatively unreliable and could possibly be improved upon by using throughput measurements or a significantly larger sample base.

In order to measure correlation a different antenna setup was required as the correlation of the triangle antennas in the above configuration was near 0 for all frequencies of interest. For the correlation a pair of 88mm monopoles with a resonance frequency at 850 MHz on a disc ground were measured inside the RC. The cross correlation was calculated from 50 pools of 1M samples from each receiver and averaged.

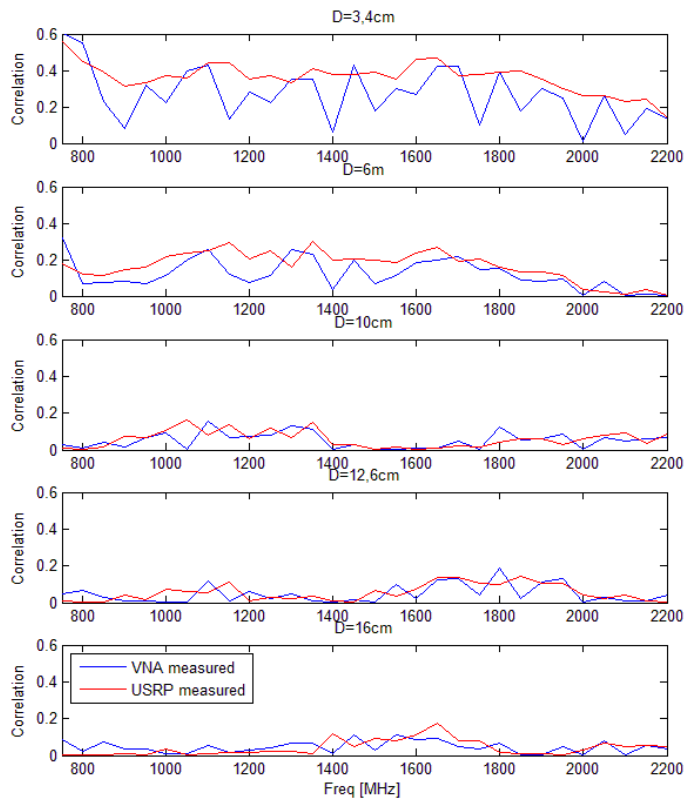


Fig. 28 USRP measured vs VNA measured correlation

As can be seen in figure 27 the measured values for diversity gain can give an idea of the scale of the diversity gain but further improvements need to be made to the measurement process or measurement setup in order to improve the accuracy of the measured data. The measured correlation in figure 28 shows good agreement with the expected value from the reference measurement using the VNA

## 4.3 Channel properties

Knowing the state of the channel is often important and can give insight into what signal behavior to expect and what parameters to choose when setting up a communication link so being able to measure those parameters is important.

### 4.3.1 Doppler spread

For measuring Doppler spread a pair of USRPs was synchronized over the MIMO link and connected to the reverberation chamber with only the reference antenna as receiving antenna and the fixed antennas as transmitting antennas. The chamber was then stepped through 200 stirrer positions and all 3 fixed antennas at each stirrer position for a total of 600 channels. At each stirrer and antenna position the channel is measured using the same channel estimation algorithm as described in equations (9-12).

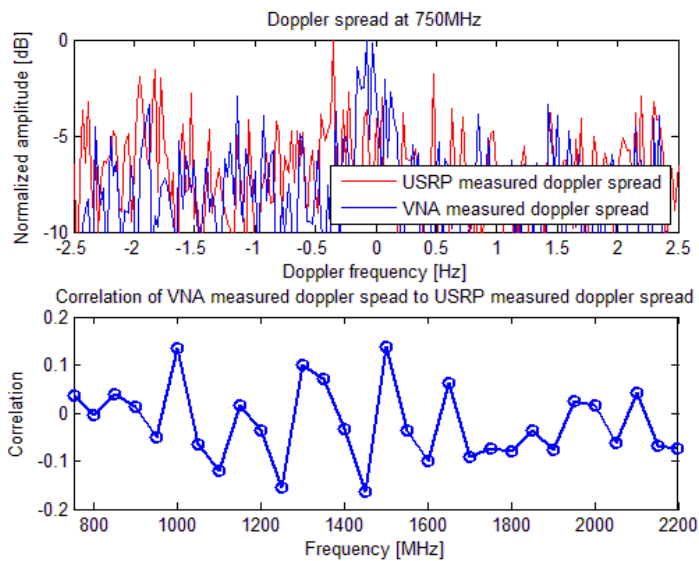


Fig. 29 Measured Doppler spread at 750 MHz by VNA and USRP and the cross correlation for all measured frequencies

As can be seen in top half of figure 29 there is little resemblance between the USRP measured Doppler spread and VNA measured Doppler spread. This is down to the USRPs phase randomness rendering it incapable of measuring the true instantaneous channel in phase. In order to verify that the data was incorrect the correlation coefficient for the two methods was calculated at each frequency and as can be seen in bottom half of figure 29 the two measured Doppler spreads are effectively uncorrelated.

Due to the random phase between initializations of the USRP the method outlined here and implemented will be hard to use as the measurements would have to be continuous for all positions to get an accurate representation of the channels inside the chamber.

### 4.3.2 Delay spread

For measuring the delay spread the SISO setup with the receiver and transmitter synchronized was used without an attenuator. With the transmitter and receiver connected directly to the RC. The antenna used was the disc cone reference antenna. To achieve a sufficiently high sampling frequency the analog to digital sampling was reduced from 16bits to 8 bits, this allows the maximum sampling frequency of 40MHz to be achieved rather than 20MHz. The measurement setup used here only achieved a sampling frequency of 33.3MHz due to limitations in network speed.

To measure the delay spread a single sample impulse was sent at the highest power available to the USRP and equations (40-42) were applied for 25 samples or 750ns after the first sample that saw the impulse. Ideally this would be done so that calculations cease once the received power is back to noise

floor levels but that proved to be wildly inaccurate at higher frequencies due to reduction in transmitted power and receiver sensitivity as shown in figure 20. This coupled with the reduced accuracy of the sampling and increased channel loss on higher frequencies resulted in an impulse peak that was only 6dB above noise floor at the receiver side

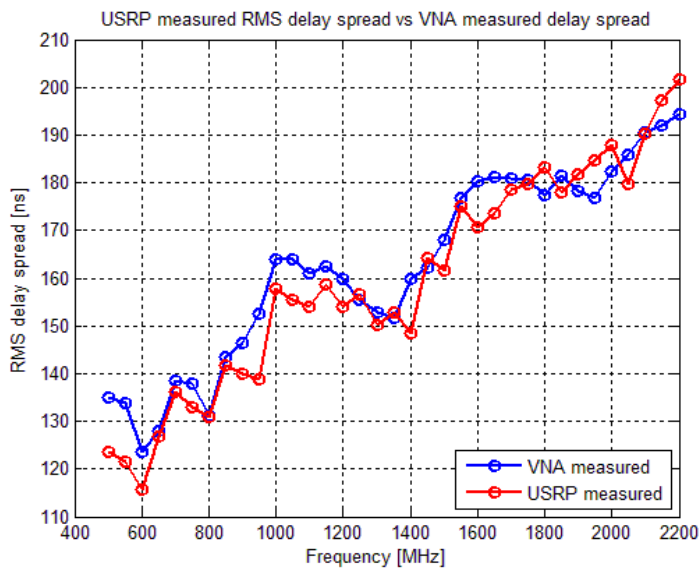


Fig. 30 USRP vs VNA measured delay spread

As can be seen in figure 30 there is very good agreement between the VNA measured and the USRP measured RMS delay spread with a maximum discrepancy of less than 15ns using the selected sampling period. This result could be further improved with an amplifier for the higher frequencies and managing to get the full sampling rate the USRP is capable of.

## 6 Conclusions

Overall it has been shown in this project that the USRP is a viable platform for a multitude of tests, measurements and algorithms in conjunction with the reverberation chamber.

It has been shown capable of measuring throughput for both single and double bit stream scenarios. This can be done without external frequency synchronization between the receiver and transmitter if there is no precoding. However, there is a requirement to use an external reference clock if precoding is to be performed to ensure that the receiver and transmitter remain constant in phase relative to each other. Therefore, the USRP can be used together with the RC to perform various test bench measurements of throughput for various systems over the RIMP channel, both simple and complex.

It is also possible to use the USRP as a network analyzer, since the received signal is near linearly related to the received power. Once calibrations of the units transmit power and receiver sensitivity are complete and suitable algorithms have been developed, it should be capable of handling most measurements that are dependent on  $S_{21}$  and  $S_{12}$  as they are dependent on the fraction of the transmitted power received and can therefore be measured by the USRP.

Measuring  $S_{11}$  and  $S_{22}$  is a challenge without external hardware as the USRP is unable to measure the reflected wave at the transmitter port. It has been shown in this project that measuring total radiated power and received power is possible with a 1dB standard deviation. There is as well potential for measuring diversity gain using the same linearity but refinement of algorithm and methods used is needed.

Both correlation and RMS delay spread can be measured accurately without any device calibration because both are functions of relative power rather than absolute.

Antenna efficiency has been shown to be measureable to within 0.3dB standard deviation over all frequencies using comparison of throughput measurements showing that it has a fairly high reliability for efficiency measurements.

While the USRP has shown itself to be a very viable test bench which offers low initial costs and great versatility, it has limitations for some applications. The largest of these are its bandwidth limitations because operation at more than 20MHz bandwidth suffers from reduced analog to digital sampling bitrate.

Further issues are slow response time when initiating transmission and reception making it unsuitable for testing over rapidly changing channels when channel state information is required at the receiver side. True channel phase estimation is as well challenging due to the random phase at which the phase locked loop locks in the hardware.

Furthermore due to significant crosstalk between transmitting and receiving port of this model of USRP used it is important to use separate units for transmission and reception of signals.

In conclusion the USRP shows promise as a test bench for both simple and advanced tests and is a promising low cost alternative to other commercial units.

## 7 References

- [1] <http://www.ni.com/usrp/>
- [2] P.S. Kildal, A. Hussain, X. Chen, C. Orlenius, A. Skårbratt, J. Åsberg, T. Svenson, T. Eriksson, "Threshold receiver model for throughput of wireless devices with MIMO and frequency diversity measured in reverberation chamber" *IEEE Antennas Wireless Propag. Lett.*, vol. 10, pp. 1201-1204, 2011
- [3] P.S. Kildal, C. Orlenius, J. Carlsson, "OTA Testing in multipath of antennas and wireless devices with MIMO and OFDM" *Proceedings of the IEEE*, Vol. 100, No. 7, July 2012
- [4] A. Hussain and P.-S. Kildal "Achieving Total Isotropic Sensitivity from Measured Throughput in Reverberation Chamber" unpublished
- [5] S. M. Alamouti "A Simple Transmit Diversity Technique for Wireless Communications" *IEEE Journal on select areas in communications*, vol. 16, no. 8, October 1998
- [6] Tse and Viswanath "Fundamentals of Wireless Communication"
- [7] <https://decibel.ni.com/content/docs/DOC-18801>
- [8] <http://www.ni.com/white-paper/13878/en/>
- [9] P.-S. Kildal, X. Chen, C. Orlenius, M. Franzén, C. Lötbäck Patané, "Characterization of Reverberation Chambers for OTA Measurements of Wireless Devices: Physical Formulations of Channel Matrix and New Uncertainty Formula", *IEEE Transactions on Antennas and Propagation*, Vol. 60, No. 8, pp. 3875-3891, Aug. 2012.
- [10] X. Chen, P. Kildal, J. Carlsson, and J. Yang, "MRC Diversity and MIMO Capacity Evaluations of Multi-Port Antennas Using Reverberation Chamber and Anechoic Chamber," *Antennas and Propagation*, *IEEE Transactions on*, vol. 61, pp. 917-926, 2013.
- [11] X. Chen, P.S. Kildal, J. Carlsson, J. Yang, "Comparison of Ergodic Capacities from Wideband MIMO Antenna Measurements in Reverberation Chamber and Anechoic Chamber", *Antennas and Wireless Propagation Letters*, vol. 10, pp. 446-449, May 2011.
- [12] X. Chen, P. S. Kildal, C. Orlenius, and J. Carlsson, "Channel Sounding of Loaded Reverberation Chamber for Over-the-Air Testing of Wireless Devices: Coherence Bandwidth Versus Average Mode Bandwidth and Delay Spread," *Antennas and Wireless Propagation Letters*, *IEEE*, vol. 8, pp. 678-681, 2009.
- [13] A. Hussain and P.S. Kildal, "Study of OTA throughput of LTE terminals for different system bandwidths and coherence bandwidths," in *Antennas and Propagation (EuCAP), 2013 7th European Conference on*, 2013, pp. 312-314.
- [14] X. Chen, P.-S. Kildal, and M. Gustafsson, "Characterization of implemented algorithm for MIMO spatial multiplexing in reverberation chamber," *IEEE Transactions on Antennas and Propagation*, vol. 61, no. 8, pp. 4400-4404, August. 2013.
- [15] P.-S. Kildal and C. Carlsson, "TCP of 20 Mobile Phones Measured in Reverberation Chamber Procedure, Results, Uncertainty and Validation" *Bluetest AB*, 4. Feb 2002
- [16] K. Rosengren and P.-S. Kildal, "Radiation efficiency, correlation, diversity gain and capacity of a six-monopole antenna array for a MIMO system: theory, simulation and measurement in reverberation chamber", *IEE Proc.-Microw. Antennas Propag.* Vol. 152, No. 1, pp 7-16 February 2005
- [17] K. Karlsson, X. Chen, P.-S. Kildal and J. Carlsson, "Doppler Spread in Reverberation Chamber Predicted From Measurements During Step-Wise Stationary Stirring", *IEEE Antennas and wireless propagation letters*, VOL. 9, pp 497-500, 2010
- [18] A. Hussain and P. Kildal, "Receiver Quality of MIMO LTE Mobile Terminals in Reverberation Chambers: Replacing TIS by OTA Throughput," 2014.
- [19] W.C. Jakes, *Microwave Mobile Communications*. 2nd ed., Wiley, 1994, pp. 45-52.
- [20] A. Paulraj, R. Nabar and D. Gore, *Introduction to space-time wireless communication*, Cambridge University Press, 2003
- [21] X. Chen and P.-S. Kildal, "Theoretical derivation and measurements of the relationship between coherence bandwidth and RMS delay spread in reverberation chamber", *EuCAP 2009*, Berlin, Germany, 2009.